AMERICAN SOCIETY FOR MICROBIOLOGY | Applied and Environmental Microbiology®

ENZYMOLOGY AND PROTEIN ENGINEERING

Phosphorothioated DNA Is Shielded from Oxidative Damage

Tianning Pu,[a] Jingdan Liang,[a] Zhiling Mei,[b] Yan Yang,[a] Jialiang Wang,[a] Wei Zhang,[a] Wei-Jun Liang,[c] Xiufen Zhou,[a] Zixin Deng,[a] Zhijun Wang[a]

[a]State Key Laboratory of Microbial Metabolism, School of Life Science and Biotechnology, Shanghai Jiao Tong University, Shanghai, People's Republic of China
[b]Institute of Plant Physiology and Ecology, Shanghai Institutes for Biological Sciences, Chinese Academy of Sciences, Shanghai, People's Republic of China
[c]Department of Life and Environmental Sciences, Faculty of Science and Technology, Bournemouth University, Poole, United Kingdom

ABSTRACT DNA is the carrier of genetic information. DNA modifications play a central role in essential physiological processes. Phosphorothioation (PT) modification involves the replacement of an oxygen atom on the DNA backbone with a sulfur atom. PT modification can cause genomic instability in *Salmonella enterica* under hypochlorous acid stress. This modification restores hydrogen peroxide (H_2O_2) resistance in the catalase-deficient *Escherichia coli* Hpx$^-$ strain. Here, we report biochemical characterization results for a purified PT modification protein complex (DndCDE) from *S. enterica*. We observed multiplex oligomeric states of DndCDE by using native PAGE. This protein complex bound avidly to PT-modified DNA. DndCDE with an intact iron-sulfur cluster (DndCDE-FeS) possessed H_2O_2 decomposition activity, with a V_{max} of 10.58 ± 0.90 mM min^{-1} and a half-saturation constant, $K_{0.5S}$, of 31.03 mM. The Hill coefficient was 2.419 ± 0.59 for this activity. The protein's activity toward H_2O_2 was observed to be dependent on the intact DndCDE and on the formation of an iron-sulfur (Fe-S) cluster on the DndC subunit. In addition to cysteine residues that mediate the formation of this Fe-S cluster, other cysteine residues play a catalytic role. Finally, catalase activity was also detected in DndCDE from *Pseudomonas fluorescens* Pf0-1. The data and conclusions presented suggest that DndCDE-FeS is a short-lived catalase. Our experiments also indicate that the complex binds to PT sites, shielding PT DNA from H_2O_2 damage. This catalase shield might be able to extend from PT sites to the entire bacterial genome.

IMPORTANCE DNA phosphorothioation has been reported in many bacteria. These PT-hosting bacteria live in very different environments, such as the human body, soil, or hot springs. The physiological function of DNA PT modification is still elusive. A remarkable property of PT modification is that purified genomic PT DNA is susceptible to oxidative cleavage. Among the oxidants, hypochlorous acid and H_2O_2 are of physiological relevance for human pathogens since they are generated during the human inflammation response to bacterial infection. However, expression of PT genes in the catalase-deficient *E. coli* Hpx$^-$ strain restores H_2O_2 resistance. Here, we seek to solve this obvious paradox. We demonstrate that DndCDE-FeS is a short-lived catalase that binds tightly to PT DNA. It is thus possible that by docking to PT sites the catalase activity protects the bacterial genome against H_2O_2 damage.

KEYWORDS DNA modification, DNA phosphorothioation, H_2O_2 decomposition, iron-sulfur cluster

DNA has a central role in cells, and DNA modifications, which occur most often at bases, are involved in fundamental physiological functions. The DNA sugar-phosphate backbone is repeating, inert, and stable, and this stability ensures the safe storage of DNA and the transmission of genetic information. The phosphorothioate (PT) modification of DNA involves the replacement of a nonbridging oxygen with sulfur in

Citation Pu T, Liang J, Mei Z, Yang Y, Wang J, Zhang W, Liang W-J, Zhou X, Deng Z, Wang Z. 2019. Phosphorothioated DNA is shielded from oxidative damage. Appl Environ Microbiol 85:e00104-19. https://doi.org/10.1128/AEM.00104-19.

Editor M. Julia Pettinari, University of Buenos Aires

Address correspondence to Zixin Deng, zxdeng@sjtu.edu.cn, or Zhijun Wang, wangzhijun@sjtu.edu.cn.

T.P. and J.L. contributed equally to this work.

Received 13 January 2019
Accepted 5 February 2019
Accepted manuscript posted online 8 February 2019
Published 4 April 2019

the DNA backbone. PT DNA can more easily resist nuclease degradation (1). As a result, synthetic PT DNA has a broad range of uses in antisense technology (2–4).

PT DNA modifications are common in different bacterial species (5, 6). In *Clostridium difficile*, the number of strains with PT may be as high as 60% (7). Five clinical isolates of *Leptospira* spp. also have DNA PT modifications (8), and PT DNA occurs in almost 50% of *Mycobacterium abscessus* strains (9, 10). These three bacteria are all human pathogens and can cause nosocomial diarrhea, leptospirosis, and chronic pulmonary disease, respectively.

PT modification is both sequence specific and stereo-specific (5, 6), and its abundance varies in different bacterial genera. In *Escherichia coli* B7A and *Salmonella enterica* serovar Cerro 87, approximately three to eight PT modifications per 10^4 nucleotides (nt) were detected (5). The highest frequency of two to three PT modifications per 10^3 nt was observed in *Vibrio* species (5). PT DNA is primarily double stranded although single-stranded DNA with PT modifications occurs (11). The recognition sequence that is modified also varies among bacteria. For example, the recognition sequences (sense/antisense [5′ to 3′]) in *E. coli* and *Streptomyces lividans* are GAAC/GTTC and GGCC/GGCC, respectively (12).

The incorporation of sulfur alters the redox and nucleophilic properties of the DNA backbone. Consequently, PT DNA is susceptible to oxidative cleavage *in vitro* (13, 14). Effective PT cleavage reagents include peracetic acid, iodine, hypochlorous acid, and hydrogen peroxide (14–16), with the latter two being of physiological relevance. Both hypochlorous acid and hydrogen peroxide are generated during human bacterial infections, and the treatment of *E. coli* and *S. enterica* with hypochlorous acid reduced their survival in a PT-dependent way (16). As a consequence of the loss in structural stability, PT modification may result in increased genome instability. Thus, it was suggested that PT may compromise the fitness of bacteria in oxidative environments (16).

Paradoxically *E. coli* Hpx$^-$ strains (H_2O_2-scavenging-enzyme deficient) have been observed to possess growth advantages under various oxidative conditions when transformed with the PT modification genes (17–19). However, the biological mechanism associated with these observations has yet to be explained. In this study, we showed that the DNA PT modification complex (DndCDE) binds strongly to PT DNA. DndCDE with an intact iron-sulfur cluster (DndCDE-FeS) is a short-lived catalase that may be able to shield PT DNA from H_2O_2 damage.

RESULTS

Fenton reaction of PT DNA. Much of the toxicity of H_2O_2 toward living organisms is due to the iron ion-dependent generation of hydroxyl radicals. In this study, we used physiological concentrations of H_2O_2 (1 mM) and Fe^{2+} (100 μM) to induce the Fenton reaction. We subsequently used high-performance liquid chromatography coupled with mass spectrometry (HPLC-MS) to examine the reaction products of synthetic PT dinucleotides with hydroxyl radicals. The results presented in Fig. 1 clearly show that the PT dinucleotide dGsA (where 's' indicates the phosphorothioate modification site) reacted readily with hydroxyl radicals, the primary oxidation products of which were the dinucleotides dGA (*m/z* 581) and H-phosphonate dG_HA (*m/z* 565) (15). H-phosphonate DNA is readily hydrolyzed under neural or basic conditions (13), and its cleavage products were also detected. However, when dGsA was separately incubated with 1 mM H_2O_2 or 100 μM $FeCl_2$, cleavage products were not detected.

Preferential complexation of DndCDE to PT DNA. The above result suggests that purified PT DNA is highly susceptible to hydroxyl radical cleavage. The results of our previous work demonstrated that the expression of DndCDE in an *E. coli* Hpx$^-$ strain (H_2O_2-scavenging-enzyme deficient) restored the H_2O_2 resistance of this strain (17) to a level that was comparable to that of the wild-type MG1655 strain (17). An explanation for this paradox is that PT sites *in vivo* may be safeguarded by an H_2O_2-degrading enzyme. To further investigate this phenomenon, we expressed the cloned *dndCDE* gene cluster from *S. enterica* serovar Cerro 87 in *E. coli*. We purified DndCDE to

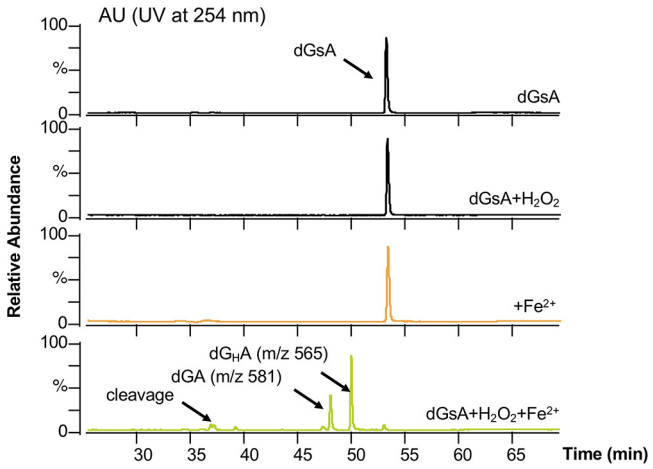

FIG 1 Phosphorothioate dinucleotide Fenton reaction. HPLC-MS analysis of PT dinucleotide dGsA reaction products in the Fenton reaction was performed. This reaction involved 1 mM H_2O_2 and 100 μM $(NH_4)_2Fe(SO_4)_2$. AU, arbitrary units.

homogeneity using a three-step procedure: Ni, heparin, and size exclusion chromatography (SEC) (Fig. 2A, panel i). We subsequently used gradient native gel electrophoresis to examine the protein complex. DndCDE did not migrate well in the native gel, appearing as a smear from approximately 440 kDa to 880 kDa (Fig. 2A, panel ii, lane 1). Cross-linking stabilized DndCDE, and the cross-linked complex appeared as multiplexed bands at approximately 440 kDa and 880 kDa and higher (Fig. 2A, panel ii, lane 2).

The binding of DndCDE to DNA was analyzed using electrophoretic mobility shift assays (EMSAs). The results presented in Fig. 2B show that, compared to unmodified

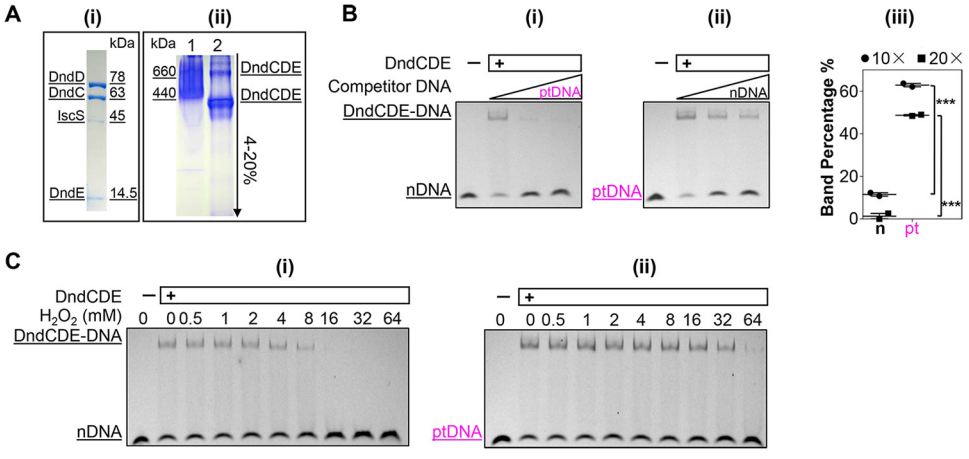

FIG 2 Binding of DndCDE to PT DNA. (A) Analysis of DndCDE using PAGE. The DndCDE complex was consecutively purified using Ni-NTA, heparin HiTrap, and Superdex 200 size exclusion columns, according to the approach described in the Materials and Methods section. The purity of DndCDE was checked using SDS-PAGE (i). Subunits (DndC/DndD/DndE) of DndCDE are labeled on the left, and the molecular weight of each subunit is labeled on the right. Gradient native gel electrophoresis of DndCDE was performed (ii). The gradient is from 4% to 20%. For lane 1, 2 μg of DndCDE protein sample was loaded directly onto the gel. For lane 2, the protein sample was cross-linked using 1 mM DSS for 20 min at room temperature and then loaded onto the gel. Ferritin protein (1 μg) was used as the size marker. (B) EMSA of DndCDE binding to DNA. PAGE was performed in a 3.96% gel in 0.5× TBE buffer. The reaction involved 3.38 μM DndCDE and 0.4 μM DNA. DNA bands were detected and recorded using an FL3000 fluorescence detector (Fujifilm Corp., Tokyo, Japan). DNA bands were quantified and analyzed using ImageJ with nonphosphorothioate DNA as the substrate and PT DNA (pink) as the competitor DNA (i) or with PT DNA as the substrate, and nonphosphorothioate DNA as the competitor DNA (ii). Quantification of the shifted DNA bands is also shown (iii). Solid circles and squares represent the results obtained when 10-fold and 20-fold quantities of competitor DNA were added, respectively. The assay was performed in triplicate. Error bars indicate standard deviations. ***, $P < 0.01$, by an unpaired t test. (C) EMSA of DndCDE binding in the presence of H_2O_2 to nonphosphorothioate DNA (i) and to PT DNA (ii). nDNA, nonphosphorothioate DNA.

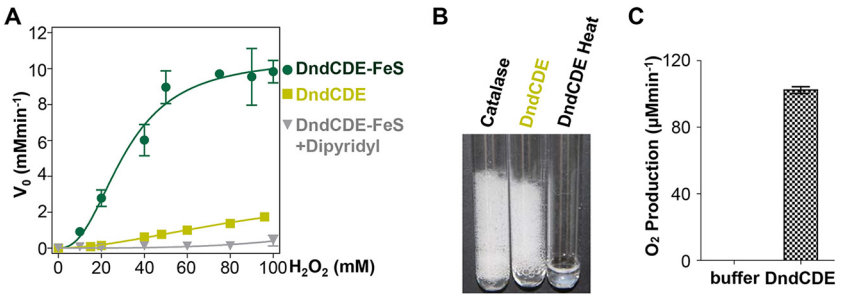

FIG 3 H_2O_2 decomposition by DndCDE or DndCDE-FeS. (A) Kinetics of H_2O_2 decomposition by DndCDE or DndCDE-FeS. H_2O_2 decomposition activity was detected via a UV absorption assay in which 1.67 μM protein was used. Increasing concentrations of H_2O_2 were used to calibrate the parameters. H_2O_2 decomposition activity of DndCDE-FeS treated with α,α-dipyridyl was also detected with different concentrations of H_2O_2. Kinetic parameters were calculated using Prism software. Error bars indicate standard deviations from three independent experiments ($n = 3$). (B) Oxygen generation during the H_2O_2 decomposition was detected using a bubble test. This analysis was performed using 10 μM DndCDE-FeS in imidazole buffer (the storage buffer plus 125 mM imidazole) supplemented with 1% Triton X-100. Boiled DndCDE-FeS and the buffer itself were used as controls. For comparison, 600 U of catalase (1896; Worthington, USA) was used as the positive control. (C) Oxygen generation was detected using a Clark-type oxygen electrode. In this assay 1.67 μM DndCDE and 50 mM H_2O_2 were used. The storage buffer was used as the negative control. Error bars indicate standard deviations from three independent experiments ($n = 3$).

DNA, PT DNA promoted DndCDE-DNA complexation. Increasing the H_2O_2 concentration decreased the binding of nonphosphorothioated DNA binding by DndCDE (Fig. 2C, panel i), and at 16 mM H_2O_2 the DNA substrate binding was completely abolished. For the PT DNA substrate, the same effect was not encountered until the concentration of H_2O_2 had reached 64 mM (Fig. 2C, panel ii). The observed binding affinity was tight and did not decrease in the presence of 32 mM H_2O_2. We concluded that DndCDE binds preferentially to PT DNA and that PT DNA complexed with DndCDE is preferentially resistant to hydrogen peroxide.

DndCDE-FeS actively decomposes H_2O_2. Fe-S clusters in Fe-S metalloproteins are well known to possess multiple and variable redox potentials that result from their possession of transition element metal atoms and their ability to adopt multiple, different oxidation states (20, 21). In addition, such enzymes are commonly involved in oxidation/reduction type reactions (22). The subunit DndC has been reported to have an iron-sulfur cluster (23), and purified DndCDE appears brownish. Thus, the Fe-S cluster of DndCDE may play a role in H_2O_2 decomposition. To further investigate this possibility, we prepared DndCDE under both aerobic and anaerobic (DndCDE-FeS) conditions. Using a UV absorption assay, we were able to detect the H_2O_2 decomposition activity of both enzymes (Fig. 3A), and both DndCDE and DndCDE-FeS were active. When DndCDE-FeS was treated with α,α'-dipyridyl, a potent metalloprotease inhibitor and a high-affinity iron chelator (24, 25), its activity was abolished. The calculated decomposition of H_2O_2 by DndCDE-FeS exhibited a V_{max} of 10.58 $\pm$ 0.90 mM min^{-1}, with a half-saturation constant, $K_{0.5S}$, of 31.03 mM (Fig. 3A) and a Hill coefficient of 2.419 $\pm$ 0.59. In contrast, the H_2O_2 decomposition by DndCDE exhibited a V_{max} of 2.09 mM min^{-1} and a H_2O_2 $K_{0.5s}$ of 58.59 mM. The plot generated from the data also fits well with the Hill equation and has a coefficient of 2.93 (Fig. 3A).

Catalase degrades H_2O_2 into water and oxygen (26). In bubble tests, we observed that H_2O_2 decomposition by DndCDE also produced a foam layer that was identical to that of catalase (Fig. 3B). The generation of oxygen during H_2O_2 decomposition by DndCDE was also measured using a Clark-type oxygen electrode (Fig. 3C). The results indicated that oxygen was one of the products of the H_2O_2 decomposition reaction.

H_2O_2 decomposition requires an intact DndCDE. To investigate whether the complexation of the three subunits in DndCDE is required for the observed H_2O_2 decomposition activity, we cloned, expressed, and purified the DndDE, DndCE, DndCD, and DndC proteins separately (see Fig. S1A in the supplemental material). The SEC step

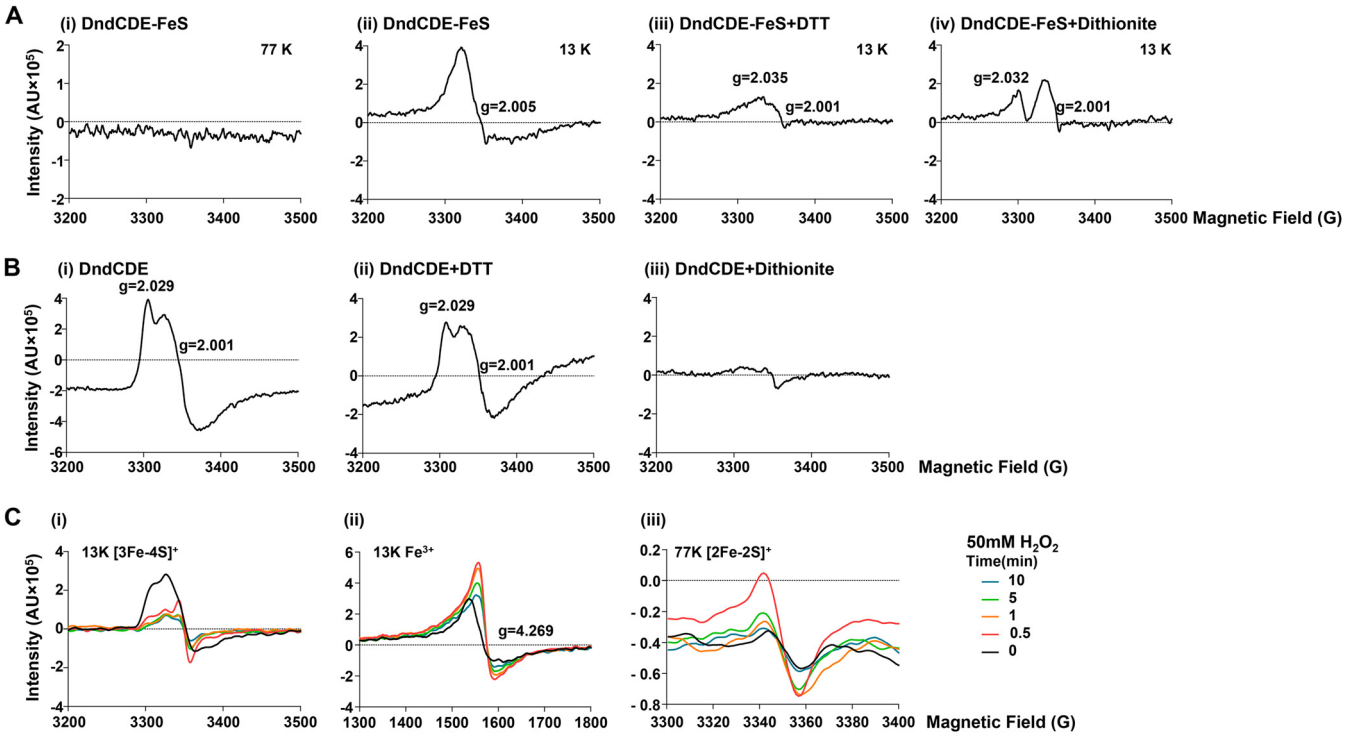

FIG 4 EPR analysis of the Fe-S cluster on DndCDE-FeS and DndCDE. EPR spectra were acquired using a Bruker EMX Plus 10/12 spectrometer. Spectra were recorded at 77 K for [2Fe-2S] clusters and at 13 K for [4Fe-4S] or [3Fe-4S] clusters. This analysis was performed using 130 μM DndCDE-FeS or DndCDE in storage buffer. The valences of [3Fe-4S] and [4Fe-4S] were determined by treating the protein sample with 2 mM dithiothreitol (DTT) and sodium dithionite. (A) EPR spectra were recorded for the following, as indicated: the Fe-S cluster on DndCDE-FeS (ii and ii), DndCDE-FeS treated with 2 mM dithiothreitol (iii), and DndCDE-FeS treated with 2 mM sodium dithionite (iv). (B) EPR spectra of the Fe-S cluster on DndCDE at 13 K were recorded for the following: DndCDE in storage buffer (i), DndCDE treated with 2 mM dithiothreitol (ii), and DndCDE treated with 2 mM sodium dithionite (iii). (C) EPR spectra of the Fe-S cluster on DndCDE treated with H_2O_2. (DndCDE was used in this assay as DndCDE-FeS generated an excessive number of bubbles that interfered with EPR detection.) For this analysis, 50 mM H_2O_2 and 130 μM DndCDE in imidazole buffer were used. The spectra were recorded after 0, 0.5, 1, 5, and 10 min of treatment, as indicated.

for the purification was not performed since these complexes were not stable on the column. We analyzed H_2O_2 decomposition using the bubble test using DndCDE and buffer as the positive and negative controls, respectively. An oxygen foam layer was observed in the tube only with the intact DndCDE, and the removal of any of the Dnd subunits abolished the observed activity (Fig. S1B). The UV absorption method was used to measure the kinetic parameters of the subcomplexes. As shown in Fig. S1C, only DndCD had significant H_2O_2 decomposition activity, but it did so with reduced V_{max} and $K_{0.5s}$ values of 1.56 mM min^{-1} and 35.5 mM, respectively, compared to values for DndCDE. DndC alone showed some very weak activity.

Fe-S cluster and H_2O_2 decomposition. In biological systems iron-sulfur (Fe-S) metalloproteins can have their Fe-S atoms arranged in a number of different ways (22). Most commonly, the clusters are organized with 2, 3, or 4 Fe atoms combined with 2 or 4 S atoms, with the three most common arrangements/configurations being 2Fe-2S, 3Fe-4S, and 4Fe-4S. In the various forms, Fe can be present as Fe^{2+} and/or Fe^{3+}. *In vivo*, Fe-S clusters are typically present as either [2Fe-2S] or [4Fe-4S] or a mixture of the two (22), with the former being less oxygen sensitive and more stable. DndCDE-FeS was used in electron paramagnetic resonance (EPR) experiments performed at 77 and 13 K to distinguish [2Fe-2S] from [4Fe-4S] (27). We observed that when EPR was performed at 77 K, there were no significant *g* value peaks (Fig. 4A, panel i), whereas at 13 K a *g* value of 2.005 was obtained, which is typical for 4Fe-4S clusters (Fig. 4A, panel ii) (27). To discern the charge state of the 4Fe-4S cluster, we treated DndCDE-FeS with either dithiothreitol or dithionite (28, 29). Dithiothreitol can reduce $[4Fe\text{-}4S]^{3+}$ to $[4Fe\text{-}4Fe]^{2+}$, whereas dithionite reduces $[4Fe\text{-}4Fe]^{2+}$ to $[4Fe\text{-}4Fe]^{+}$ (29) We observed that when the protein was treated with dithiothreitol, the peak characteristic of $[4Fe\text{-}4S]^{3+}$ was

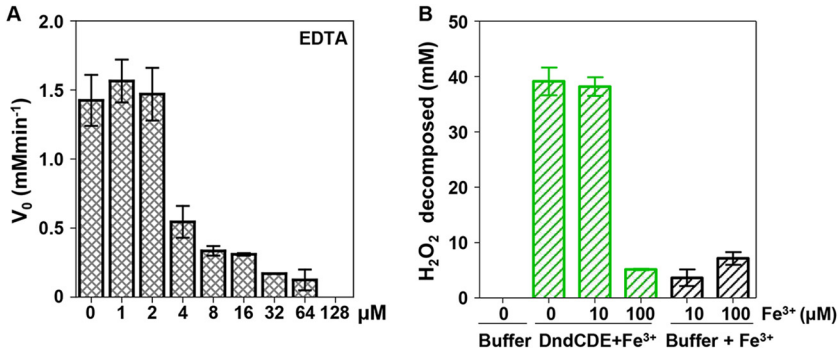

FIG 5 Effects of EDTA and ferric ions on H_2O_2 decomposition by DndCDE. (A) Initial velocity (V_0) of H_2O_2 decomposition by DndCDE in the presence of increasing concentrations of EDTA. (B) H_2O_2 decomposition in the presence of ferric ion. Decomposition was detected using a colorimetric assay since ferric ion interferes with UV detection. Imidazole buffer was used as a control. Standard deviations were calculated from three independent experiments ($n = 3$).

abolished, and only residual resonances, with *g* values of 2.035 and 2.001, remained (Fig. 4A, panel iii). Treatment with dithionite led to the appearance of two peak signals with *g* values of 2.032 and 2.001 (Fig. 4A, panel iv), suggesting the presence of the $[4Fe\text{-}4S]^+$ configuration (27, 30).

When DndCDE was analyzed by EPR, no significant *g* value peaks at 77 K were observed (data not shown), whereas at 13 K, two peak signals were detected with *g* values of 2.029 and 2.002 (Fig. 4B, panel i). Although the treatment of DndCDE with dithiothreitol was not observed to reduce the signal, the treatment with dithionite did significantly reduce signal intensity (Fig. 4B, panels ii and iii). Taken together, these results suggested that non-dithionite-treated DndCDE possessed an Fe-S cluster in the $[3Fe\text{-}4S]^+$ configuration (29) that was reduced by dithionite to $[3Fe\text{-}4S]^0$.

EPR was also used in experiments designed to follow the state of the Fe-S cluster during the DndCDE decomposition of H_2O_2, the results of which are shown in Fig. 4C (panels i to iii). The results showed that the EPR signal corresponding to the $[4Fe\text{-}4S]^+$ state quickly decreased after the initiation of the H_2O_2 decomposition reaction over the first 30 s and remained steady for the duration of the reaction (10 min) (Fig. 4C, panel i). In contrast, the Fe^{3+} signal, with a *g* value of 4.3, approximately doubled during the first 30 s of the reaction and then gradually fell back to its initial value over the next 9.5 min (Fig. 4C, panel ii). A weak signal for $[2Fe\text{-}2S]^+$ was detected at 30 s that subsequently decreased slightly and then remained constant for approximately 5 min (Fig. 4C, panel iii).

DndCDE H_2O_2 decomposition activity does not depend on ferric ion. The above EPR experimental results indicated that the iron-sulfur cluster on DndCDE was damaged by H_2O_2, with Fe^{3+} generated simultaneously. We suspected that the Fe^{3+} generated in the reaction may play a role in the H_2O_2 decomposition reaction through the Fenton reaction (31). EDTA is known to damage the functionality of Fe-S clusters through the chelation of iron ions (32, 33). In contrast, EDTA contributes to the generation of hydroxyl in the EDTA-Fe(III)/H_2O_2 Fenton-like system (34). We analyzed the influence of EDTA on the H_2O_2 decomposition activity of DndCDE using a UV absorbance method, the results of which are shown in Fig. 5A. The H_2O_2 decomposition activity of DndCDE decreased as the concentration of EDTA increased, and at a concentration of 128 μM EDTA, the enzymatic activity was abolished.

To further confirm that ferric ions do not participate in catalyzing the H_2O_2 decomposition reaction, ferric ions were added to the reaction mixture. The reaction was performed using a colorimetric assay since ferric ions interfere with UV absorbance. The results presented in Fig. 5B show that in the presence of 10 μM ferric ions, no increase in DndCDE activity was observed. In contrast, in the presence of 100 μM ferric ions, the H_2O_2 decomposition activity of DndCDE was reduced to background levels. Thus,

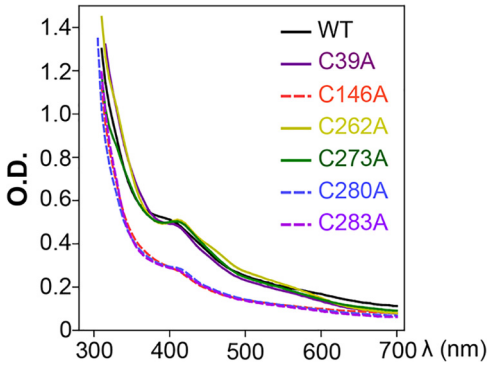

FIG 6 Characterization of cysteine-to-alanine DndC mutants. Individually, each cysteine residue in DndC of DndCDE was mutated to alanine. Purified DndC mutants were scanned using UV-Vis to detect the characteristic Fe-S absorbance peak (λ_{400}). For efficient scanning, the proteins were concentrated to 130 μM.

we concluded that the H_2O_2 decomposition activity of DndCDE is dependent on the iron-sulfur cluster rather than on Fe^{3+}.

Conserved cysteine residues in DndC participate in H_2O_2 decomposition. The above results suggested that the DndC subunit of DndCDE is responsible for the observed H_2O_2 decomposition activity and not DndDE or DndE. Because of the indicated importance of DndC in the H_2O_2 activity associated with PT, we conducted an *in silico* analysis on the amino acid sequence of DndC. The results of this analysis indicated that the *S. enterica* DndC protein possesses six cysteine residues (Cys^{39}, Cys^{146}, Cys^{262}, Cys^{273}, Cys^{280}, and Cys^{283}) and that all of these residues except Cys^{39} are highly conserved in DndC homologues from other organisms (Fig. S2). Consequently, we conducted a series of experiments in which the cysteine residues of the DndC subunit were sequentially replaced with alanines to study the involvement of each residue in H_2O_2 decomposition.

UV-visible light (UV-Vis) spectroscopy was used to investigate the state of the Fe-S cluster in the various *dndC* cysteine mutants of DndCDE, and the results are shown in Fig. 6. The results clearly show that the DndC C39A, C262A, and C273A mutants retained the wild-type absorbance profiles between 400 and 420 nm, whereas only a slight shoulder (i.e., small peak) was observed for the other three mutants (Fig. 6).

When the DndCDE variants possessing the *dndC* mutations were analyzed for their ability to decompose H_2O_2 by UV absorption, the results clearly showed that, except for the Cys^{39} mutant, the cysteine variants abolished H_2O_2 decomposition activities (Fig. S3).

Cysteine is the most common residue used in iron coordination although other amino acid residues, such as histidine and arginine, are also observed to coordinate iron-sulfur clusters (35, 36). Our results showed that Cys^{146}, Cys^{280}, and Cys^{283} are needed for Fe-S coordination in DndC and support the conclusion that the Fe-S cluster is involved in the H_2O_2 decomposition activity of DndCDE. Although Cys^{262} and Cys^{273} did not appear to be involved in Fe-S cluster coordination, they are required for the H_2O_2 decomposition activity of DndCDE. In contrast, Cys^{39} does not appear to be essential for DndCDE H_2O_2 decomposition activity or to be involved in Fe-S coordination.

H_2O_2 decomposition activity of DndCDE from *Pseudomonas fluorescens* Pf0-1. We also overexpressed the *dnd* gene cluster from *Pseudomonas fluorescens* Pf0-1 in *E. coli*. We purified DndCDE of strain Pf0-1 ($DndCDE_{Pf0}$) using the same three-step protocol described earlier (Fig. S4A). The UV-Vis spectrum of $DndCDE_{Pf0}$ showed optical absorbance between 400 and 420 nm (Fig. S4B), which is typical for Fe-S clusters. We then assayed the H_2O_2 decomposition activity using a bubble test. Fig. S4C shows that oxygen bubbles were generated by $DndCDE_{Pf0}$.

DISCUSSION

In *E. coli* and *S. enterica*, it has been shown that there are approximately 1,400 PT modifications per genome (5), with an average distance of approximately 3.4 kb between modifications. Since it has been classically believed that PT modification renders DNA more vulnerable to degradation and damage, such modification could potentially cause genome instability (16) and would therefore be considered to be disadvantageous.

Bacteria that are pathogenic toward humans, such as *Salmonella enterica*, live in particularly challenging oxidative environments (37, 38) that occur partly as a consequence of the inflammatory response processes induced by infection in the host organism. In particular, superoxide, hydrogen peroxide, hydroxyl radicals, and other reactive oxygen species (ROS) are generated by phagocytic cells (39) as part of the inflammatory response, and phosphorothioated DNA is paradoxically especially susceptible to cleavage by hydroxyl radicals at physiological concentrations via the Fenton reaction (Fig. 1). Consequently, the observation that PT modifications have biochemical activity in many microorganisms (6, 40), including those involved in infection, seems counterintuitive. However, the fact that the *dndCDE* genes are widespread among prokaryotic organisms, from those involved in infectious disease to bacteria living in hot springs (17), strongly suggests that PT confers a biological advantage. A possible explanation could be that the DNA PT modification is accompanied by localized free radical scavenging activity, particularly in microorganisms involved in infectious disease. Reactive oxygen species can present in a number of different forms depending upon local conditions and environment, and if the above hypothesis is correct, it seems possible that the substrate specificity of specific DndCDEs may be tailored to take these differences into account. Notably, DndCDE from the soil-dwelling bacterium *Pseudomonas fluorescens* Pf0-1 also has H_2O_2 decomposition activity (see Fig. S4A in the supplemental material). Interestingly, for *S. enterica*, redundant H_2O_2 scavengers (three catalases and two alkyl hydroperoxide reductases) can contribute to its virulence and oxidative stress resistance (41). Furthermore, reactive oxygen species generated during inflammation promote *S. enterica* serovar Typhimurium outgrowth in the gut lumen (42).

The Hill coefficient of 2.4 (Fig. 3A) measured in this study suggests that the H_2O_2 decomposition activity of DndCDE-FeS is subject to allosteric regulation, and the K_m of DndCDE-FeS for H_2O_2 is approximately 31 mM ($K_{0.5s}$) (Fig. 3A). This concentration may be physiologically relevant to H_2O_2 decomposition (Fig. 2C and 3A).

Fe-S clusters are known to participate in sensing oxidative stress (28, 43), and Fe-S cluster- containing proteins are also involved in the hydrogen peroxide-scavenging reaction. IsF from *Methanosarcina thermophila* contains one 4Fe-4S center (44) that has been shown to reduce O_2 and H_2O_2. Hybrid cluster proteins (HCPs) contain two types of Fe-S clusters, $[4Fe\text{-}4S]^{2+/1+}$ and $[2Fe\text{-}2S]^{2+/1+}$. HCPs have roles in the oxidative stress defense, and HCPs from *E. coli* and *Desulfovibrio desulfuricans* exhibit peroxidase activity (45). In this study, we showed that the Fe-S cluster in DndC is involved in catalyzing the H_2O_2 decomposition reaction. The Fe-S cluster in DndC is susceptible to H_2O_2 damage. In the presence of H_2O_2, the Fe-S cluster signal was sustained for more than 5 min (Fig. 4C, panel i). Thus, the catalase activity of DndCDE appears to be short-lived.

Bacterial DNA is bound by numerous bacterial chromatin proteins (46). In *E. coli*, the proteins HU, H-NS (histone-like nucleoid structuring protein), Fis, MatP, ParB, integration host factor (IHF), and SMC (structural maintenance of chromosome) bend, stiffen, and bridge chromatin into high-order structures (47, 48). These proteins compact genomic DNA nearly 1,000-fold to accommodate it to a confined volume. There are multiple levels of chromatin organization, from 10-kbp domains to 0.5- to 1.5-Mbp macrodomains (47). DNA PT modification has been shown to enhance the affinity of DNA-binding proteins (49–51), and PT sites in bacterial DNA are also potentially bound by proteins *in vivo*. In this study, we observed that DndCDE preferentially bind to PT DNA (Fig. 2B and C). Interestingly, the DndD protein in DndCDE shows high similarity

TABLE 1 Bacterial strains and plasmids

Strain or plasmid	Description	Reference or source
Strains		
Salmonella enterica serovar Cerro 87	Strain contains the *dndBCDE* gene cluster with modification site at GAAC/GTTC	60
Escherichia coli DH10B	F^- Δ*mcrA* (*mrr-hsdRMS-mcrBC*), cloning vector	Invitrogen
Escherichia coli BL21(DE3)	*E. coli* B strain with DE3, a λ prophage carrying the T7 RNA polymerase gene; host strain for protein hetero-expression	Stratagene
Plasmids		
pET-28a (+)	pBR322 origin, expression vector, Kan^r	Novagen
pET-15b	pBR322 origin, expression vector, Amp^r	Novagen
$pDndBCDE_H$	Derived from pET-28a, with DNA region coding DndBCDE inserted at NcoI-XhoI sites, enables the host DNA phosphorothioation, Kan^r	52
$pDndBCD_H$	Derived from $pDndBCDE_H$, with in-frame deletion in *dndE*, Kan^r	52
$pDndBCE_H$	Derived from $pDndBCDE_H$, with in-frame deletion in *dndD*, Kan^r	52
$pDndBDE_H$	Derived from $pDndBCDE_H$, with in-frame deletion in *dndC*, Kan^r	52
$pDndBC_H$	Derived from pET-28a, with DNA region coding DndBC, Kan^r	52
pIscS	Derived from pET-15b, with *iscS* gene and N-terminal His tag, Amp^r	This lab
pDnd-DndC-C39A	$pDndBCDE_H$ derivative, site mutant with C39A on DndC, Kan^r	This study
pDnd-DndC-C146A	$pDndBCDE_H$ derivative, site mutant with C146A on DndC, Kan^r	This study
pDnd-DndC-C262A	$pDndBCDE_H$ derivative, site mutant with C262A on DndC, Kan^r	This study
pDnd-DndC-C273A	$pDndBCDE_H$ derivative, site mutant with C273A on DndC, Kan^r	This study
pDnd-DndC-C280A	$pDndBCDE_H$ derivative, site mutant with C280A on DndC, Kan^r	This study
pDnd-DndC-C283A	$pDndBCDE_H$ derivative, site mutant with C283A on DndC, Kan^r	This study

to SMC proteins (6). Presumably, the binding of DndD increases chromosome compaction or avoids chromosome uncoiling. When docked to the approximately 1,400 PT sites in bacterial genomes, DndCDEs could potentially form a catalase shield, covering each of the 10-kbp chromatin domains and safeguarding the entire genome from H_2O_2 damage.

MATERIALS AND METHODS

Bacterial strains, plasmids, and culture conditions. Bacterial strains and plasmids used in this work are listed in Table 1, and most have been described in previous publications (52). Specifically, the *dndC* C39A, C146A, C262A, C273A, C280A, and C283A mutants were generated using gene-specific primers (Table 2) to amplify the entire $pDndBCDE_H$ plasmid. Primers possessed a 19-nt 5′ primer extension to facilitate cyclization of the PCR product in *E. coli*, and the 3-bp *dndC* modified sequence used in the creation of the *dndC* mutant was placed in the middle of the 5′ primer extension. PCR products were digested with DpnI (Thermo Fisher Scientific, Inc., MA, USA) for 4 h to remove the methylated plasmid

TABLE 2 Primers and DNA fragments[a]

Oligonucleotide function and name	Sequence (5′→3′)
Site-directed mutagenesis	
C39A-S	GAATTTATGCGGCGGATAAGCGTCCGTGGGTAATTGG
C39A-A	TTATCCGCCGCATAAATTCTTTGAACCTCAGCAACAT
C146A-S	TTCGCTGGGCGACCGAGCGTATGAAAATCAATCCGGT
C146A-A	CGCTCGGTCGCCCAGCGAAAACTACGGGTTGGGGCCG
C262A-S	AGGGTGAGGCGCCCCTGGTGATCGACGAAAGTACCCC
C262A-A	ACCAGGGGCGCCTCACCCTGTGCGGAAGAATCCATAT
C273A-S	CCCCCTCTGCGGGGAACTCTCGCTTTGGCTGCTGGAC
C273A-A	GAGTTCCCCGCAGAGGGGGTACTTTCGTCGATCACCA
C280A-S	GCTTTGGCGCGTGGACCTGTACCGTAGTCACCAAAGA
C280A-A	CAGGTCCACGCGCCAAAGCGAGAGTTCCCGCAAGAGG
C283A-S	GCTGGACCGCGACCGTAGTCACCAAAGATAAAGCGAT
C283A-A	ACTACGGTCGCGGTCCAGCAGCCAAAGCGAGAGTTCC
Electrophoresis mobility shift assay	
24 bp-ds-GA/GT (sense)	CCTCTTGCGGGAACTCTCGCTTTG
24 bp-ds-GA/GT (antisense)	CAAAGCGAGAGTTCCCGCAAGAGG
24 bp-ds-G**s**A/G**s**T (sense)	CCTCTTGCGGG**s**AACTCTCGCTTTG
24 bp-ds-G**s**A/G**s**T (antisense)	CAAAGCGAGAG**s**TTCCCGCAAGAGG

[a]The lowercase boldface "s" indicates the phosphorothioate modification site. Underlining indicates the sequence of interest.

template, and the resulting unmethylated PCR amplification product was purified using an AxyPrep DNA gel extraction kit (Axygen, Corning, NY, USA). PCR product identities were confirmed by size determination in 1% agarose gels using a DNA size marker for comparison (Invitrogen 1 Kb Plus DNA ladder; Thermo Fisher Scientific, Inc.). Once product identity had been confirmed, the desired fragment was stabilized by transformation into *E. coli* strain DH10B using the protocol of Inoue et al. (53). For heterologous gene expression experiments, the *dndC* mutant plasmid was isolated and purified using an AxyPrep plasmid extraction kit (Axygen Corning) and transformed into *E. coli* strain BL21(DE3)/plysS (Agilent Technologies, CA, USA).

Bacterial cells were routinely cultured in Luria broth medium (10 g/liter tryptone, 5 g/liter yeast extract, 10 g/liter sodium chloride) supplemented with 50 μg ml^{-1} kanamycin when needed for strain selection. Specifically, *E. coli* strains used in protein expression experiments were grown in 1 liter of LB medium containing 50 μg ml^{-1} kanamycin at 37°C with shaking at 250 rpm until the culture optical density at 600 nm (OD_{600}) reached 0.6. At this point gene expression was induced by addition of isopropyl-D-thiogalactopyranoside (IPTG) to a final concentration of 0.1 mM, and the culture was allowed to incubate for a further 24 h at 16°C. After this, cells were harvested by centrifugation at 6,000 $\times$ *g* for 20 min and, if not used immediately in protein purification, stored flash-frozen at −80°C.

Protein expression and purification. (i) N-terminal His-tagged cysteine desulfurase, IscS. The recovery and purification of N-terminal His-tagged cysteine desulfurase followed the general protocol described by Xiong et al. (52) in which 1 g of cell pellet or frozen cell pellet was resuspended in 50 ml of lysis buffer (20 mM Tris-HCl, pH 8.0, 150 mM NaCl, and 5% glycerol) in a sterile 50-ml polypropylene centrifuge tube (Corning, NY, USA) and sonicated on ice at 100 W using a 6.4-mm-diameter probe for a total of 10 min with 2-s bursts and 4-s intervals (Qsonica Sonicator Q500: Qsonica Sonicators, Newtown, Canada). Subsequently, insoluble cell debris was removed by centrifugation at 18,000 $\times$ *g* for 20 min, and the supernatant was then applied to a 1-ml Ni-nitrilotriacetic acid (NTA) column (GE Life Sciences, MA, USA), which was washed with 10 ml of Ni wash buffer (20 mM Tris-HCl, pH 8.0, 150 mM NaCl, 40 mM imidazole, and 5% glycerol). Bound protein was then eluted with 5 ml of Ni elution buffer 2 (20 mM Tris-HCl, pH 8.0, 150 mM NaCl, 500 mM imidazole, and 5% glycerol), and 2.5 ml of the eluate was desalted using a PD-10 desalting column (GE Life Sciences, MA, USA) with 3.5 ml of storage buffer (20 mM Tris-HCl, pH 8.0, 150 mM NaCl, 5% glycerol) according to the manufacturer's instructions. The desalted protein solution was then subjected to a Bradford assay (54).

(ii) C-terminal His-tagged Dnd protein complex DndCDE or $DndCDE_{Pfo}$. The recovery and purification of DndCDE (or $DndCDE_{Pfo}$) protein complex involved taking 5 g of cell pellet or frozen cell pellet and resuspending the cells in 25 ml of lysis buffer (20 mM Tris-HCl, pH 8.0, 150 mM NaCl, and 5% glycerol) in a sterile 50-ml polypropylene centrifuge tube (Corning). The cell suspension was then treated in an identical manner to that described for the extraction of IscS protein except that the entire volume eluted from the Ni-NTA column was loaded onto a 1-ml heparin high-performance column (HiTrap; GE Life Sciences), which was washed with five column bed volumes (CBV) of heparin wash buffer 1 (20 mM Tris-HCl, pH 8.0, 25 mM NaCl, and 5% glycerol) followed by five CBV of heparin wash buffer 2 (20 mM Tris-HCl, pH 8.0, 150 mM NaCl, and 5% glycerol). Protein was subsequently eluted with 5 ml of heparin elution buffer (20 mM Tris-HCl, pH 8.0, 500 mM NaCl, and 5% glycerol), and the eluate was subjected to size exclusion chromatography on an ÄKTA fast protein liquid chromatography system (GE Life Sciences) using a preequilibrated Superdex 200 10/30 column (GE Life Sciences) in heparin wash buffer 2. Eluate was collected in 1-ml fractions which were monitored for their absorbance at a wavelength of 280 nm (λ_{280}). Pooled peak fractions (3 ml) with the highest absorbance reading were collected and concentrated to 0.5 ml using a centrifugal filter at 8,000 $\times$ g and 4°C for 2 h (Amicon Ultra, Merck, Darmstadt, Germany). Concentrated, purified protein was then dialyzed in 1 liter of storage buffer (20 mM Tris-HCl, pH 8.0, 150 mM NaCl, 5% glycerol) for 6 h at 4°C, and the resulting DndCDE protein was quantified by Bradford assay (54).

(iii) Gradient native gel electrophoresis detection of both native and cross-linked DndCDE. The preparation of cross-linked DndCDE was achieved by treatment with 1 mM disuccinimidyl suberate (DSS) (Thermo Fisher Scientific, Inc., MA, USA) for 20 min at room temperature (55).

The 4% to 20% gradient native gel was prepared according to the protocol described by Wittig et al. (56). Basically, 4% acrylamide and 20% acrylamide were prepared separately on ice. Four percent acrylamide contained 1.2 ml of acrylamide-bisacrylamide mixture (total concentration of the monomers acrylamide and bisacrylamide [T], 49.5%; concentration of the cross-linker [C] relative to the total concentration 3% [Solarbio, Beijing, China]), 5 ml of 3$\times$ Tris-glycine buffer (75 mM Tris base and 57.6 mM glycine), 100 μl of 10% (wt/vol) ammonium persulfate (APS), 10 μl of tetramethylethylenediamine (TEMED), and 8.7 ml of water. Twenty percent acrylamide contained 6 ml of acrylamide-bisacrylamide mixture (49.5% T, 3% C; Solarbio, Beijing, China), 5 ml of 3$\times$ Tris-glycine buffer (75 mM Tris base and 57.6 mM glycine), 3 ml of glycerol, 75 μl of 10% (wt/vol) APS, 7.5 μl of TEMED, and 918 μl of water. Gradient was achieved by adding 20% acrylamide into 4% acrylamide while the latter solution was also pumped into the vertical electrophoresis apparatus with a peristaltic pump. Two micrograms of protein sample was used for detection. One microgram of ferritin protein (A600457-0500; Sangon Biotech, Shanghai, China) was used as the size marker.

(iv) *In vitro* anaerobic enzymatic formation of active Fe-S cluster Dnd protein complex, DndCDE-FeS. The formation of active DndCDE-FeS was performed under anaerobic conditions (nitrogen) in a glove box (Coy Laboratory Product, Inc., MI, USA) in a reaction catalyzed by IscS (23). Typically, 20 μM DndCDE was incubated for 30 min at room temperature under aerobic conditions with 1 mM α,α'-dipyridyl and 2 mM dithionite, after which the reaction mixture was desalted using a PD-10 desalting column (GE Life Sciences) according to the manufacturer's instructions, and 3.5 ml of eluate

was concentrated to approximately 900 μl by centrifugation in a 0.5-ml centrifugal filter at 8,000 $\times$ *g* and 4°C for 2 h (Amicon Ultra; Merck, Darmstadt, Germany). From this point onward, all other steps were undertaken under anaerobic conditions. The concentrated protein (20 μM) was then mixed with 20 μM purified IscS protein, 7.5 mM dithiothreitol, 0.5 mM $Fe(NH_4)_2(SO_4)_2$, and 0.5 mM cysteine in storage buffer (20 mM Tris-HCl, pH 8.0, 150 mM NaCl, 5% glycerol) in a total volume of 1 ml, and the sample tubes were sealed and incubated at 4°C overnight. Subsequently, the mixture was centrifuged at 15,000 $\times$ *g* for 10 min, and the supernatant was desalted by passage through a PD-10 desalting column (GE Life Sciences) and concentrated by centrifugation in a 0.5-ml centrifugal filter (Centricon Plus-20 [PL-10]; Millipore, MA, USA) at 4°C. Finally, the tube containing DndCDE-FeS was sealed with Parafilm before being removed from the glove box. The protein was used in the experiments immediately.

UV-Vis and EPR analysis of DndCDE and DndCDE-FeS. The UV-visible light (UV-Vis) absorption characteristics of the DndCDE protein and its Cys mutants were investigated using a microtiter plate reader (BioTek Synergy 2; BioTek Instruments, Inc., VT, USA) equipped with Gen5 software. Briefly a 200-μl sample containing 130 μM, 20 mg ml, of the protein complex in storage buffer (20 mM Tris-HCl, pH 8.0, 150 mM NaCl, 5% glycerol) in a 96-well microplate (3599; Corning, NY, USA) was scanned for its absorption between λ_{290} and λ_{700}. This concentration of protein complex was used as it had previously been determined to be the minimum required to produce a visible spectroscopic peak for the Fe-S cluster.

Electron spin resonance (EPR) spectrum acquisitions were performed under aerobic conditions, and in these experiments 130 μM DndCDE in storage buffer (20 mM Tris-HCl, pH 8.0, 150 mM NaCl, 5% glycerol) was used. Protein was supplemented with either sodium dithionite (2 mM) or dithiothreitol (2 mM) where appropriate. EPR spectra were acquired using a Bruker EMX Plus 10/12 spectrometer (Bruker Co., Ltd., Bremen, Germany) equipped with an Oxford ESR910 liquid helium continuous-flow cryostat (Oxford Instrument Co., Ltd., Oxfordshire, UK) and Bruker WINEPR software at the National High Magnetic Field Laboratory of the Chinese Academy of Sciences (Hefei, China). Conditions used for EPR signal acquisition were the following: microwave frequency, 9.387 GHz; field modulation amplitude, 5 gauss; microwave power, 2 mW; modulation frequency, 100 kHz at either 13 K or 77 K.

EPR was also used in experiments designed to determine the possible difference in the Fe-S cluster states of DndCDE proteins during their reactions with H_2O_2. In this case 1,200 μl of DndCDE solution (130 μM in the storage buffer) was mixed with 12 μl of 5 M H_2O_2 and 60 μl of 2.5 M imidazole, pH 8.0. Samples (200 μl) of the mixture were removed into EPR tubes and snap-frozen in liquid nitrogen after 0.5 min, 1 min, 2 min, 5 min, and 10 min in readiness for EPR data acquisition, which was performed in a manner identical to that described above.

Fenton reaction and HPLC-MS detection of phosphorothioate DNA. The 100-μl reaction mixture contained 25 μM dGsA (synthesized from Sangon Biotech, Shanghai, China) and 100 μM $FeCl_2$. A final concentration of 1 mM H_2O_2 (from 100 mM stock) was added to initiate the Fenton reaction (31). The reaction was performed at room temperature for 30 min. Then 10 μl of the reaction solution was loaded onto a YMC-C_{18} reverse-phase column (250 mm by 4.6 mm; 5-μm particle size; YMC Co., Ltd., Kyoto, Japan) fitted to an Agilent 1100 series LC/MSD (liquid chromatography/mass-selective detector) trap system. Sample separation was achieved by use of a two-solvent mixture (solvent A consisting of 0.1% acetic acid in water and solvent B consisting of 0.1% acetic acid in acetonitrile) at a flow rate of 0.4 ml/min and a temperature of 30°C. Gradient conditions were 1% to 13% solvent B for 35.5 min, 13% to 30% solvent B for 20 min, and finally 1% solvent B for 10 min. UV absorption was monitored at $\lambda_{254.4}$. Ionization was set in positive mode, gas flow was 10 liters min^{-1}, nebulizer pressure was 30 lb/in^2, drying gas temperature was 325°C, and capillary voltage was 3,100 V. Signals at *m/z* 597 (dGsA), 565 (dG_HA), and 581 (dGA) were extracted to confirm the identities of the main peaks.

EMSAs. DNA sequences used in electrophoresis mobility shift assays (EMSAs) are listed in Table 2; they were purchased from Genewiz (Jiangsu, China) and were either labeled with 5′ 6-carboxyfluorescein (FAM) and/or phosphorothioated at their GA/GT residues. The DNA fragments were prepared as 500-μl volumes which contained 50 μl of 400 μM sense and antisense oligonucleotides, 100 μl of 5$\times$ annealing buffer (150 mM Tris-HCl, pH 8.0, 50 mM $MgCl_2$, and 240 mM NaCl), and 300 μl of water. Prior to use, these mixtures were heated to 100°C for 10 min and then slowly cooled to room temperature. The DNA solutions were then either used immediately or stored frozen until required.

Each 20-μl EMSA mixture contained 2 μl of a specific 5′ FAM-labeled oligonucleotide (4 μM), 2 μl or 4 μl (4 μM) of complementary oligonucleotide where required, 2 μl of binding buffer (100 mM Tris-HCl, pH 8.0, 1 M KCl, 1 mM dithiothreitol, 0.1 mg ml^{-1} bovine serum albumin [BSA], and 50% glycerol) along with 10 μl of 6.67 μM DndCDE and sterile double-distilled water to make up the volume. Mixtures were incubated at room temperature for 40 min, and then 10 μl was subjected to PAGE in a 3.96% gel (49.5% T and 3% C, acrylamide-bisacrylamide [Solarbio, Beijing, China]) in 0.5$\times$ TBE buffer (44.5 mM Tris, 44.5 mM boric acid, 1 mM EDTA). The gel was electrophoresed at 100 V for 1 h after which DNA bands were detected and recorded using an FL3000 fluorescence detector (Fujifilm Corp., Tokyo, Japan).

Measurement of DndCDE and DndCDE-FeS H_2O_2 decomposition activities. (i) Colorimetric assay. H_2O_2 scavenging activity was assayed in a 100-μl reaction mixture composed of 20 mM Tris-HCl, pH 8.0, 150 mM NaCl, 125 mM imidazole, 5% glycerol, and 40 mM H_2O_2 (Sangon Biotech). Scavenging reactions were initiated by addition of 1.67 μM (0.25 mg ml^{-1}) protein and incubated at 25°C for a total of 20 min. Ten-microliter aliquots were removed from the reaction mixtures at 5-min intervals and diluted 1,000-fold with storage buffer (20 mM Tris-HCl, pH 8.0, 150 mM NaCl, 5% glycerol) to a final volume of 10 ml. Twenty microliters of the diluted reaction mixture was then added to 200 μl of ferric-xylenol orange assay mixture (Hydrogen Peroxide Quantitative Assay kit; Sangon Biotech) (18, 57), and the mixture was allowed to rest at room temperature for 30 min, after which its optical density was measured

at λ_{595}. To investigate the impact of Fe^{2+}, 10 μM or 100 μM $FeCl_2$ was added into the assay prior to H_2O_2. All reactions were carried out in triplicate.

(ii) Bubble test. Bubble tests (26) were performed to follow the liberation of oxygen during the decomposition of H_2O_2 in a qualitative fashion by the two proteins. In this assay the presence of Triton X-100 entraps bubbles of oxygen liberated during the reaction at its surface to form a foam layer which is photographed after 10 min. Reaction volumes were 1 ml and contained 10 μM protein, 3 M H_2O_2, 20 mM Tris-HCl, pH 8.0, 150 mM NaCl, 125 mM imidazole, 5% glycerol, and 1% Triton X-100. This concentration of H_2O_2 was chosen based on the report of Iwase et al. (26) as it is the concentration required to produce bubbles and foam, which can be entrapped at the reaction's surface by the surfactant; two negative controls were used for comparison. The first involved the use of heat-inactivated protein, and the second consisted of reaction buffer alone.

(iii) UV absorption. The H_2O_2 decomposition rates of DndCDE and DndCDE-FeS were also measured in real time in a 96-well UV-transparent microplate (Corning) using a Synergy2 microplate reader (BioTek Instruments, Inc., VT) operated at λ_{240} (H_2O_2 has a characteristic absorption peak at λ_{240}) (58). Concentrations of H_2O_2 employed were 0, 15, 20, 24, 30, 40, 48, 60, 80, 96, 120, 160, 200, and 240 mM, and scavenging reaction mixtures (100-μl total volume) were composed of 20 mM Tris-HCl, pH 8.0, 150 mM NaCl, 125 mM imidazole, 5% glycerol, and 1.67 μM protein. All assays were performed in triplicate and initiated by addition of H_2O_2. Readings were taken at 3-s intervals over a period of 2 min, and the concentration of H_2O_2 remaining in solution was calculated by reference to a standard curve constructed previously from a known concentration series of H_2O_2. The concentration of DndCDE-FeS was half that of DndCDE, and experiments involving the use of DndCDE-FeS were terminated at 1 min, in both cases because the large volume of oxygen generated would interfere detection. Calculations relating to H_2O_2 decomposition were made using Prism 5 software (GraphPad Software, Inc., CA, USA). To investigate the impact of EDTA, 1 μM, 2 μM, 4 μM, 8 μM, 16 μM, 32 μM, 64 μM, or 128 μM EDTA was added into the assay prior to H_2O_2.

(iv) O_2 liberation rate measurement (pO_2 oxygen electrode). Rate measurement of oxygen liberation during DndCDE H_2O_2 decomposition was also undertaken using a Clark-type oxygen electrode as described by Jacoby et al. (59). (This experiment also served to confirm that the gas generated on H_2O_2 decomposition was oxygen). Reaction mixtures (2-ml total volume) were composed of 50 mM H_2O_2 and 1.67 μM DndCDE in storage buffer supplemented with 125 mM imidazole (pH 8.0). Partial O_2 pressure (pO_2) measurement was terminated when the oxygen concentration reached saturation level, and all reactions were carried out in triplicate.

SUPPLEMENTAL MATERIAL

Supplemental material for this article may be found at https://doi.org/10.1128/AEM.00104-19.

SUPPLEMENTAL FILE 1, PDF file, 0.2 MB.

ACKNOWLEDGMENTS

We thank Gong-Li Tang for his generous support in providing the anaerobic box for the study. We thank Yuanhua and Jin Wenbing from Tang Gong-Li's group for their guidance in performing the anaerobic protein purification and Tong Wei, Yu Lu, and Zou Youming (National High Magnetic Field Laboratory of the Chinese Academy of Sciences, Hefei, China) for EPR operation and data collection. We also thank the core facility of the School of Life Science and Biotechnology for the help with HPLC-MS.

This work was supported by the Ministry of Science and Technology (973 program, grant 2015CB554203) and the National Science Foundation of China (grants 31470830, 21661140002, and 91753123).

REFERENCES

1. Vosberg HP, Eckstein F. 1982. Effect of deoxynucleoside phosphorothioates incorporated in DNA on cleavage by restriction enzymes. J Biol Chem 257:6595–6599.
2. Eckstein F. 2000. Phosphorothioate oligodeoxynucleotides: what is their origin and what is unique about them? Antisense Nucleic Acid Drug Dev 10:117–121. https://doi.org/10.1089/oli.1.2000.10.117.
3. Zhang Y, Lin A, Zhang C, Tian Z, Zhang J. 2014. Phosphorothioate-modified CpG oligodeoxynucleotide (CpG ODN) induces apoptosis of human hepatocellular carcinoma cells independent of TLR9. Cancer Immunol Immunother 63:357–367. https://doi.org/10.1007/s00262-014-1518-y.
4. Lee J, Byeon SE, Jung JY, Kang MH, Park YJ, Jung KE, Bae YS. 2015. Azasugar-containing phosphorothioate oligonucleotide (AZPSON) DBM-2198 inhibits human immunodeficiency virus type 1 (HIV-1) replication by blocking HIV-1 gp120 without affecting the V3 region. Mol Cells 38:122–129. https://doi.org/10.14348/molcells.2015.2129.
5. Wang L, Chen S, Vergin KL, Giovannoni SJ, Chan SW, DeMott MS, Taghizadeh K, Cordero OX, Cutler M, Timberlake S, Alm EJ, Polz MF, Pinhassi J, Deng Z, Dedon PC. 2011. DNA phosphorothioation is widespread and quantized in bacterial genomes. Proc Natl Acad Sci U S A 108:2963–2968. https://doi.org/10.1073/pnas.1017261108.
6. Zhou X, He X, Liang J, Li A, Xu T, Kieser T, Helmann JD, Deng Z. 2005. A novel DNA modification by sulphur. Mol Microbiol 57:1428–1438. https://doi.org/10.1111/j.1365-2958.2005.04764.x.
7. Alonso R, Martín A, Peláez T, Marín M, Rodríguez-Creixéms M, Bouza E. 2005. An improved protocol for pulsed-field gel electrophoresis typing of *Clostridium difficile*. J Med Microbiol 54:155–157. https://doi.org/10.1099/jmm.0.45808-0.
8. Ribeiro RL, Machry L, Brazil JM, Ramos TM, Avelar KE, Pereira MM. 2009. Technical improvement to prevent DNA degradation of *Leptospira* spp. in pulsed field gel electrophoresis. Lett Appl Microbiol 49:289–291. https://doi.org/10.1111/j.1472-765X.2009.02641.x.

9. Zhang Y, Yakrus MA, Graviss EA, Williams-Bouyer N, Turenne C, Kabani A, Wallace RJ, Jr. 2004. Pulsed-field gel electrophoresis study of *Mycobacterium abscessus* isolates previously affected by DNA degradation. J Clin Microbiol 42:5582–5587. https://doi.org/10.1128/JCM.42.12.5582-5587.2004.
10. Howard ST, Newman KL, McNulty S, Brown-Elliott BA, Vasireddy R, Bridge L, Wallace RJ, Jr. 2013. Insertion site and distribution of a genomic island conferring DNA phosphorothioation in the *Mycobacterium abscessus* complex. Microbiology 159:2323–2332. https://doi.org/10.1099/mic.0.070318-0.
11. Cao B, Chen C, DeMott MS, Cheng Q, Clark TA, Xiong X, Zheng X, Butty V, Levine SS, Yuan G, Boitano M, Luong K, Song Y, Zhou X, Deng Z, Turner SW, Korlach J, You D, Wang L, Chen S, Dedon PC. 2014. Genomic mapping of phosphorothioates reveals partial modification of short consensus sequences. Nat Commun 5:3951. https://doi.org/10.1038/ncomms4951.
12. Liang J, Wang Z, He X, Li J, Zhou X, Deng Z. 2007. DNA modification by sulfur: analysis of the sequence recognition specificity surrounding the modification sites. Nucleic Acids Res 35:2944–2954. https://doi.org/10.1093/nar/gkm176.
13. Zhou X, Deng Z, Firmin JL, Hopwood DA, Kieser T. 1988. Site-specific degradation of *Streptomyces lividans* DNA during electrophoresis in buffers contaminated with ferrous iron. Nucleic Acids Res 16:4341–4352. https://doi.org/10.1093/nar/16.10.4341.
14. Ray T, Mills A, Dyson P. 1995. Tris-dependent oxidative DNA strand scission during electrophoresis. Electrophoresis 16:888–894. https://doi.org/10.1002/elps.11501601149.
15. Xie X, Liang J, Pu T, Xu F, Yao F, Yang Y, Zhao YL, You D, Zhou X, Deng Z, Wang Z. 2012. Phosphorothioate DNA as an antioxidant in bacteria. Nucleic Acids Res 40:9115–9124. https://doi.org/10.1093/nar/gks650.
16. Kellner S, DeMott MS, Cheng CP, Russell BS, Cao B, You D, Dedon PC. 2017. Oxidation of phosphorothioate DNA modifications leads to lethal genomic instability. Nat Chem Biol 13:888–894. https://doi.org/10.1038/nchembio.2407.
17. Yang Y, Xu G, Liang J, He Y, Xiong L, Li H, Bartlett D, Deng Z, Wang Z, Xiao X. 2017. DNA backbone sulfur-modification expands microbial growth range under multiple stresses by its anti-oxidation function. Sci Rep 7:3516. https://doi.org/10.1038/s41598-017-02445-1.
18. Dai D, Du A, Xiong K, Pu T, Zhou X, Deng Z, Liang J, He X, Wang Z. 2016. DNA phosphorothioate modification plays a role in peroxides resistance in *Streptomyces lividans*. Front Microbiol 7:1380. https://doi.org/10.3389/fmicb.2016.01380.
19. Wu T, Huang Q, Wang XL, Shi T, Bai L, Liang J, Wang Z, Deng Z, Zhao YL. 2017. Mechanistic investigation on ROS resistance of phosphorothioated DNA. Sci Rep 7:42823. https://doi.org/10.1038/srep42823.
20. Kiley PJ, Beinert H. 2003. The role of Fe-S proteins in sensing and regulation in bacteria. Curr Opin Microbiol 6:181–185. https://doi.org/10.1016/S1369-5274(03)00039-0.
21. Beinert H, Kiley PJ. 1999. Fe-S proteins in sensing and regulatory functions. Curr Opin Chem Biol 3:152–157. https://doi.org/10.1016/S1367-5931(99)80027-1.
22. Johnson DC, Dean DR, Smith AD, Johnson MK. 2005. Structure, function, and formation of biological iron-sulfur clusters. Annu Rev Biochem 74:247–281. https://doi.org/10.1146/annurev.biochem.74.082803.133518.
23. You D, Wang L, Yao F, Zhou X, Deng Z. 2007. A novel DNA modification by sulfur: DndA is a NifS-like cysteine desulfurase capable of assembling DndC as an iron-sulfur cluster protein in *Streptomyces lividans*. Biochemistry 46:6126–6133. https://doi.org/10.1021/bi602615k.
24. Ashmun RA, Look AT. 1990. Metalloprotease activity of CD13/aminopeptidase N on the surface of human myeloid cells. Blood 75:462–469.
25. Jin A, Lee JN, Kim MS, Kwak S, Kim SJ, Song K, Choe SK, Park R. 2016. 2,2′-Dipyridyl induces pexophagy. Biochem Biophys Res Commun 469:941–947. https://doi.org/10.1016/j.bbrc.2015.12.098.
26. Iwase T, Tajima A, Sugimoto S, Okuda K, Hironaka I, Kamata Y, Takada K, Mizunoe Y. 2013. A simple assay for measuring catalase activity: a visual approach. Sci Rep 3:3081. https://doi.org/10.1038/srep03081.
27. Hsueh KL, Yu LK, Chen YH, Cheng YH, Hsieh YC, Ke SC, Hung KW, Chen CJ, Huang TH. 2013. FeoC from Klebsiella pneumoniae contains a [4Fe-4S] cluster. J Bacteriol 195:4726–4734. https://doi.org/10.1128/JB.00687-13.
28. Crack JC, Green J, Thomson AJ, Le Brun NE. 2014. Iron-sulfur clusters as biological sensors: the chemistry of reactions with molecular oxygen and nitric oxide. Acc Chem Res 47:3196–3205. https://doi.org/10.1021/ar5002507.
29. Zanello P. 2018. Structure and electrochemistry of proteins harboring iron-sulfur clusters of different nuclearities. Part II. [4Fe-4S] and [3Fe-4S] iron-sulfur proteins. J Struct Biol 202:250–263. https://doi.org/10.1016/j.jsb.2018.01.010.
30. Netz DJ, Stith CM, Stumpfig M, Kopf G, Vogel D, Genau HM, Stodola JL, Lill R, Burgers PM, Pierik AJ. 2011. Eukaryotic DNA polymerases require an iron-sulfur cluster for the formation of active complexes. Nat Chem Biol 8:125–132. https://doi.org/10.1038/nchembio.721.
31. Winterbourn CC. 1995. Toxicity of iron and hydrogen peroxide: the Fenton reaction. Toxicol Lett 82-83:969–974. https://doi.org/10.1016/0378-4274(95)03532-X.
32. Nishio K, Nakai M. 2000. Transfer of iron-sulfur cluster from NifU to apoferredoxin. J Biol Chem 275:22615–22618. https://doi.org/10.1074/jbc.C000279200.
33. Jin Z, Heinnickel M, Krebs C, Shen G, Golbeck JH, Bryant DA. 2008. Biogenesis of iron-sulfur clusters in photosystem I: holo-NfuA from the cyanobacterium *Synechococcus* sp. PCC 7002 rapidly and efficiently transfers [4Fe-4S] clusters to apo-PsaC in vitro. J Biol Chem 283:28426–28435. https://doi.org/10.1074/jbc.M803395200.
34. Engelmann MD, Bobier RT, Hiatt T, Cheng IF. 2003. Variability of the Fenton reaction characteristics of the EDTA, DTPA, and citrate complexes of iron. Biometals 16:519–527. https://doi.org/10.1023/A:1023480617038.
35. Koehler C, Carlier L, Veggi D, Balducci E, Di Marcello F, Ferrer-Navarro M, Pizza M, Daura X, Soriani M, Boelens R, Bonvin AM. 2011. Structural and biochemical characterization of NarE, an iron-containing ADP-ribosyltransferase from Neisseria meningitidis. J Biol Chem 286:14842–14851. https://doi.org/10.1074/jbc.M110.193623.
36. Berkovitch F, Nicolet Y, Wan JT, Jarrett JT, Drennan CL. 2004. Crystal structure of biotin synthase, an S-adenosylmethionine-dependent radical enzyme. Science 303:76–79. https://doi.org/10.1126/science.1088493.
37. Aussel L, Zhao W, Hebrard M, Guilhon AA, Viala JP, Henri S, Chasson L, Gorvel JP, Barras F, Meresse S. 2011. *Salmonella* detoxifying enzymes are sufficient to cope with the host oxidative burst. Mol Microbiol 80:628–640. https://doi.org/10.1111/j.1365-2958.2011.07611.x.
38. Oberley-Deegan RE, Rebits BW, Weaver MR, Tollefson AK, Bai X, McGibney M, Ovrutsky AR, Chan ED, Crapo JD. 2010. An oxidative environment promotes growth of *Mycobacterium abscessus*. Free Radic Biol Med 49:1666–1673. https://doi.org/10.1016/j.freeradbiomed.2010.08.026.
39. Imlay JA. 2008. Cellular defenses against superoxide and hydrogen peroxide. Annu Rev Biochem 77:755–776. https://doi.org/10.1146/annurev.biochem.77.061606.161055.
40. Ou HY, He X, Shao Y, Tai C, Rajakumar K, Deng Z. 2009. *dnd*DB: a database focused on phosphorothioation of the DNA backbone. PLoS One 4:e5132. https://doi.org/10.1371/journal.pone.0005132.
41. Hebrard M, Viala JP, Meresse S, Barras F, Aussel L. 2009. Redundant hydrogen peroxide scavengers contribute to *Salmonella* virulence and oxidative stress resistance. J Bacteriol 191:4605–4614. https://doi.org/10.1128/JB.00144-09.
42. Winter SE, Thiennimitr P, Winter MG, Butler BP, Huseby DL, Crawford RW, Russell JM, Bevins CL, Adams LG, Tsolis RM, Roth JR, Baumler AJ. 2010. Gut inflammation provides a respiratory electron acceptor for Salmonella. Nature 467:426–429. https://doi.org/10.1038/nature09415.
43. Crack JC, Thomson AJ, Le Brun NE. 2017. Mass spectrometric identification of intermediates in the O_2-driven [4Fe-4S] to [2Fe-2S] cluster conversion in FNR. Proc Natl Acad Sci U S A 114:E3215–E3223. https://doi.org/10.1073/pnas.1620987114.
44. Cruz F, Ferry JG. 2006. Interaction of iron-sulfur flavoprotein with oxygen and hydrogen peroxide. Biochim Biophys Acta 1760:858–864. https://doi.org/10.1016/j.bbagen.2006.02.016.
45. Almeida CC, Romao CV, Lindley PF, Teixeira M, Saraiva LM. 2006. The role of the hybrid cluster protein in oxidative stress defense. J Biol Chem 281:32445–32450. https://doi.org/10.1074/jbc.M605888200.
46. Rocha EP. 2008. The organization of the bacterial genome. Annu Rev Genet 42:211–233. https://doi.org/10.1146/annurev.genet.42.110807.091653.
47. Dame RT, Tark-Dame M. 2016. Bacterial chromatin: converging views at different scales. Curr Opin Cell Biol 40:60–65. https://doi.org/10.1016/j.ceb.2016.02.015.
48. Badrinarayanan A, Le TB, Laub MT. 2015. Bacterial chromosome organization and segregation. Annu Rev Cell Dev Biol 31:171–199. https://doi.org/10.1146/annurev-cellbio-100814-125211.
49. Crooke ST, Wang S, Vickers TA, Shen W, Liang XH. 2017. Cellular uptake

and trafficking of antisense oligonucleotides. Nat Biotechnol 35:230–237. https://doi.org/10.1038/nbt.3779.
50. Liang XH, Sun H, Shen W, Crooke ST. 2015. Identification and characterization of intracellular proteins that bind oligonucleotides with phosphorothioate linkages. Nucleic Acids Res 43:2927–2945. https://doi.org/10.1093/nar/gkv143.
51. Anderson KM, Esadze A, Manoharan M, Bruschweiler R, Gorenstein DG, Iwahara J. 2013. Direct observation of the ion-pair dynamics at a protein-DNA interface by NMR spectroscopy. J Am Chem Soc 135:3613–3619. https://doi.org/10.1021/ja312314b.
52. Xiong W, Zhao G, Yu H, He X. 2015. Interactions of Dnd proteins involved in bacterial DNA phosphorothioate modification. Front Microbiol 6:1139. https://doi.org/10.3389/fmicb.2015.01139.
53. Inoue H, Nojima H, Okayama H. 1990. High efficiency transformation of *Escherichia coli* with plasmids. Gene 96:23–28. https://doi.org/10.1016/0378-1119(90)90336-P.
54. Bradford MM. 1976. A rapid and sensitive method for the quantitation of microgram quantities of protein utilizing the principle of protein-dye binding. Anal Biochem 72:248–254. https://doi.org/10.1016/0003-2697(76)90527-3.
55. Assil-Kishawi I, Abou-Samra AB. 2002. Sauvagine cross-links to the second extracellular loop of the corticotropin-releasing factor type 1 receptor. J Biol Chem 277:32558–32561. https://doi.org/10.1074/jbc.M204964200.
56. Wittig I, Braun HP, Schagger H. 2006. Blue native PAGE. Nat Protoc 1:418–428. https://doi.org/10.1038/nprot.2006.62.
57. Gay CA, Gebicki JM. 2002. Perchloric acid enhances sensitivity and reproducibility of the ferric-xylenol orange peroxide assay. Anal Biochem 304:42–46. https://doi.org/10.1006/abio.2001.5566.
58. Nelson DP, Kiesow LA. 1972. Enthalpy of decomposition of hydrogen peroxide by catalase at 25 degrees C (with molar extinction coefficients of H_2O_2 solutions in the UV). Anal Biochem 49:474–478. https://doi.org/10.1016/0003-2697(72)90451-4.
59. Jacoby RP, Millar AH, Taylor NL. 2015. Assessment of respiration in isolated plant mitochondria using Clark-type electrodes. Methods Mol Biol 1305:165–185. https://doi.org/10.1007/978-1-4939-2639-8_12.
60. Xu T, Yao F, Zhou X, Deng Z, You D. 2010. A novel host-specific restriction system associated with DNA backbone S-modification in *Salmonella*. Nucleic Acids Res 38:7133–7141. https://doi.org/10.1093/nar/gkq610.